Rotational State-Specific Dynamics of SiF $C^2\Delta-B^2\Sigma^+$ Collision-Induced Transfer

Neil A. Jackson, Colin J. Randall, and Kenneth G. McKendrick*

Department of Chemistry, The University of Edinburgh, The King's Buildings, Edinburgh EH9 3JJ, U.K.

Received: September 2, 1997; In Final Form: October 28, 1997[⊗]

Laser excitation on the $C^2\Delta-X^2\Pi$ transition was used to prepare discrete rotational levels of the SiF $C^2\Delta$, $v = 0$ state, allowing their state-specific collisional behavior to be investigated. Time- and wavelength-resolved returning C−X fluorescence spectra established that the initial populations were only partially perturbed by rotationally inelastic processes within the $C^2\Delta$ state at the typical pressures of our experiments. Transfer within the F_1 manifold appears to be favored by a factor of ∼2 over transfer from F_1 to F_2. There is relatively little dependence on rotational state (in the range $j = 2.5-21.5$) of the rate constant for total collisional removal of the $C^2\Delta$ state by either H_2 or N_2. As previously established, a fraction of the collisionally removed population is deposited in the lower-lying $B^2\Sigma^+$ state. Dispersed B−X fluorescence spectra revealed broad rotational distributions in the predominant $B^2\Sigma^+$, $v' = 0$ product level in collisions with H_2 and N_2, indicating substantial release of rotational energy during the transfer between electronic states. There is a positive correlation between the peak and average product j' and the initial rotational state j. The main features of the observed behavior are reproduced by a limiting impulsive model. We believe this to be a consequence of the respective valence and Rydberg characters of the $C^2\Delta$ and $B^2\Sigma^+$ states.

1. Introduction

Interelectronic state collisional quenching is a potentially important process whenever electronically excited molecules are produced under conditions where the number density makes the rate of collisions competitive with the radiative rate. Typical environments of this type would include those prevailing in combustion, regions of the atmosphere, plasmas, discharges, certain laser gain media, etc.

The proper understanding and modeling of such systems require not only a knowledge of the total collisional removal rates of the excited species, which have historically been quite extensively examined, but also of the detailed branching over the possible product levels. These measurements are, in general, significantly more challenging and correspondingly far fewer have been performed, even for the simplest case of diatomic molecules.

The state of this field has recently been comprehensively reviewed by Dagdigian.[1] Although considerable progress has been achieved, largely through laser-based spectroscopic techniques, several important and fundamental questions have not been fully answered. There is still active inquiry into the factors that control the vibronic product state distributions and in particular the role of the Franck−Condon overlap and vibronic energy deficit between initial and product levels.[1] As a prime example, several extended series of experiments have focused on the isoelectronic $A^2\Pi-X^2\Sigma^+$ transitions in N_2^+,[2−7] CN,[8−16] and CO^+ [17−21] induced by interactions with rare gases. This detailed and systematic work has been complemented by advanced theoretical treatments.[13−25] The calculations are very successful in some respects, particularly for the rotational propensities (see below). However, even for these best-studied cases, there remain serious discrepancies between measured and calculated vibrational branching ratios.[13,24,25] Theory is unable to account for the observed relatively efficient transfer over large energy gaps. This type of behavior can be even more extreme, with the dominant channels involving large vibronic energy gaps and effectively no population being transferred to near-degenerate levels, such as in collision-induced NH($a^1\Delta-X^3\Sigma^-$) transitions.[26−28]

In the majority of examples so far investigated, relatively small changes in rotational state, Δj, are found to accompany the change in electronic state.[1] A variety of limiting models, which have been applied to systems such as alkali dimers,[29,30] reproduce this behavior. The detailed calculations for the N_2^+−He and CN−He systems introduced above[13,24,25] successfully predict not only the small Δj propensity but also subtle details of fine structure state partitioning. However, there are some notable exceptions to the otherwise generally low level of rotational energy release, including NH ($c^1\Pi-A^3\Pi$) transitions induced by a variety of partners.[31]

Finally, a third respect in which different systems exhibit a diversity of behavior for reasons that are not fully understood is the role of spectroscopic perturbations between states of the isolated molecules.[1] The extent to which these act as "gateway" levels, with enhanced *collisional* transfer probabilities, has been found to vary considerably. However, it is clear that such perturbations are not a prerequisite for efficient collisional coupling, because they are strictly absent (for symmetry reasons) from some systems that nevertheless exhibit substantial collision-induced transfer rates.

In this paper, we advance what is known about collisional transfer between specific pairs of excited states in the silicon halides,[32,33] and in particular the SiF $C^2\Delta-B^2\Sigma^+$ system.[34,35] We believe this to be a topic of considerable current interest in the context of the discussion above because it simultaneously provides examples of efficient transfer over large vibronic energy gaps and of substantial Δj values accompanying a collision-induced electronic transition. (We note also that there

* To whom correspondence should be addressed. E-mail: K.McKendrick@ed.ac.uk.

[⊗] Abstract published in *Advance ACS Abstracts,* December 15, 1997.

S1089-5639(97)02840-5 CCC: $15.00
Published on Web 01/01/1998

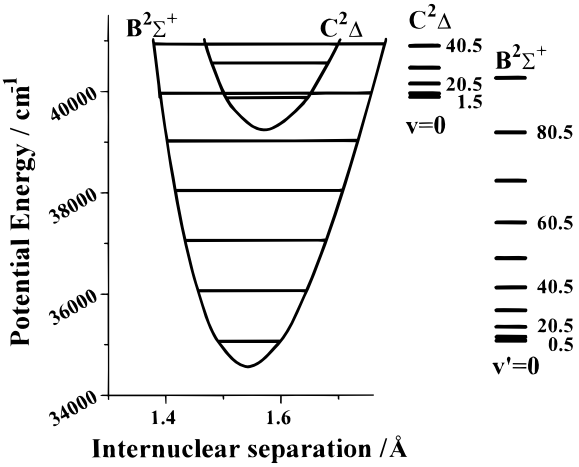

Figure 1. Potential energy curves and selected rovibronic energy levels for the SiF $C^2\Delta$ and $B^2\Sigma^+$ states. The position of every 10th rotational level in $v = 0$ of each state is indicated.

will be no low-order perturbations between $^2\Delta$ and $^2\Sigma^+$ states in the absence of a collision partner and therefore no influence of gateway levels.)

Collisional coupling of the SiCl $B'^2\Delta$ and $B^2\Sigma^+$ states was first studied at the vibronic level by Jeffries.[32] Subsequent work in our own group[33] extended the range of quenchers examined at this level, and also included the first, limited information on rotational branching. The product vibrational distributions and electronic branching fraction were found to be remarkably sensitive to the identity of the quencher.

We went on to study the nominally analogous SiF $C^2\Delta-B^2\Sigma^+$ system and found[34] some stark contrasts with the behavior for SiCl. The dominant vibronic channels from SiF $C^2\Delta$ $v = 0$ and 1 involve $\Delta v = 0$ and, therefore, surprisingly large vibronic energy gaps of $\sim$5000 cm^{-1}, as illustrated in Figure 1. Unlike SiCl, these propensities closely match the Franck−Condon overlap between $C^2\Delta$ and $B^2\Sigma^+$ vibrational wave functions and are correspondingly relatively independent of the identity of the quencher. Most recently, we presented[35] the first details of rotational effects in SiF $C^2\Delta-B^2\Sigma^+$ transfer, with excitation at two different bandheads used to prepare initial $C^2\Delta$ state populations characterized by distinctly different average *j* states. These initial results indicated that a significant fraction of the vibronic energy deficit is partitioned to SiF rotation.

The current study is an advance over the previous work because we have now managed to prepare individual initial rotational levels of the SiF $C^2\Delta$ state, which, as we shall show, are only moderately affected by collisional rotational redistribution. This allows a more quantitative assessment of the correlations between initial and final states in the SiF $C^2\Delta-B^2\Sigma^+$ transfer process. We also present the first measurements of the rotational level dependence of the SiF $C^2\Delta$ state total quenching rate constant. We compare these new results with the predictions of a limiting, impulsive kinematic model, which we describe in more detail than previously.[35] We conclude by discussing the relationship between the apparent success of this impulsive mechanism and the electronic characters of the states involved.

2. Experimental Section

The experimental approach was essentially the same as that described in detail previously,[34,35] with a few technical modifications. In essence, ground-state SiF $X^2\Pi$ radicals were generated in a discharge−flow system by microwave discharge in a mixture of SiF_4 and Ar. A second independent flow of a quenching gas (H_2, N_2, Ar, etc.) was added downstream of the discharge inlet and upstream of the observation point. Since our previous measurements,[34,35] we have carried out a careful recalibration of the flow characteristics of the system, which has allowed a significant improvement in the accuracy of absolute quenching rate constants. The total pressure was measured near the observation zone (MKS Baratron, Type 627) and maintained typically in the range 1−5 Torr by a high throughput mechanical pump (Edwards E2M80).

Laser-induced fluorescence (LIF) signals were excited at the observation point by the output of a pulsed, tunable dye laser system (Spectron Laser Systems dye laser (SL4000G) and mixing−doubling unit (SL4000D−SL4000EX) pumped by the third harmonic of a Nd:YAG laser (SL803)). The fluorescence was collected perpendicular to the laser beam and flow axes by a system of lenses, dispersed through a monochromator (Hilger and Watts, Monospek 1000, 1 m focal length, UV-blazed grating) and detected by a photomultiplier (EMI 9558QB or EMI 9789QB). Signals were preamplified (EMI A2 or Stanford Research Systems SR 240), captured by a transient digitizer (DSP Technologies 2001A, 100 MHz), and passed via a CAMAC (IEEE 583) databus to a microcomputer for processing. The microcomputer also controlled other experimental variables, such as the scanning of the dye laser and the monochromator, via appropriate CAMAC modules.

The following gases were used directly from the suppliers, with the manufacturers' stated purities as indicated: Ar (BOC), 99.998%; H_2 (BOC), 99.99%; N_2 (BOC), 99.99%; and SiF_4 (Union Carbide), 99.99%, (Fluorochem), 99.5%.

3. Results

3.1. Rotational State Preparation in the $C^2\Delta$ State. The relevant spectroscopy of the SiF C−X and B−X systems has been described in detail previously.[36] In this paper, we concentrate on rotational effects during transfer from the $C^2\Delta$ $v = 0$ level to the predominant $v' = 0$ level of the $B^2\Sigma^+$ product.[34] The potential curves and associated energy defects are shown in Figure 1.

An experimental LIF excitation spectrum of the $^2\Delta-^2\Pi_{1/2}$ subband of the C−X (0,0) transition is presented in Figure 2. As can be seen from this figure, at the available dye-laser resolution, the spectral congestion in the region to the short wavelength side of the $^QP_{21} + Q_1$ bandhead would make the excitation of individual C state rotational levels very difficult. However, the isolated P_1 branch to longer wavelength is more suitable, at least for relatively low levels not too close to the P_1 bandhead and neglecting the unresolved Λ-doubling in the C state. The positions of the lines we have used for the *j*-selected experiments are marked in Figure 2. At the penalty of lower signal sizes, this is an improvement in rotational discrimination over our previous report[35] where excitation at the respective $^QP_{21} + Q_1$ and P_1 bandheads was used to prepare contrasting but inevitably rather extended initial distributions.

3.2. Inelastic Processes within the C State. Our primary aim was to study interelectronic state collisional transfer. Nevertheless, there is some possibility of competitive inelastic transfer *within* the initial state. The relative influence of such interfering processes can be restricted by ensuring that the product of the total pressure and the effective time scale is kept sufficiently low. This leads to the standard compromise between strict "single-collision" conditions and the magnitude of the desired, collisionally induced signal.

Fortunately, we could independently assess the degree of inelastic redistribution within the C state by collecting dispersed,

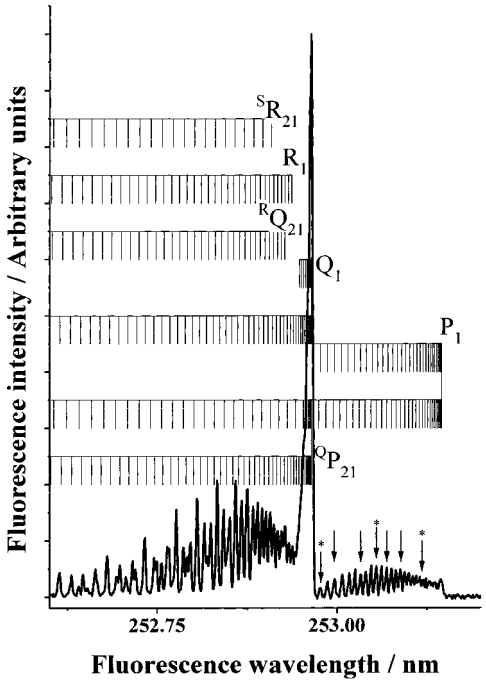

Figure 2. Experimental SiF $C^2\Delta-X^2\Pi_{1/2}$ (0,0) LIF excitation spectrum. The positions of individual lines within the P_1 branch that were pumped in *j*-selective experiments are indicated by arrows; those with asterisks were used to measure decay constants, and the remainder to investigate rotational population distributions.

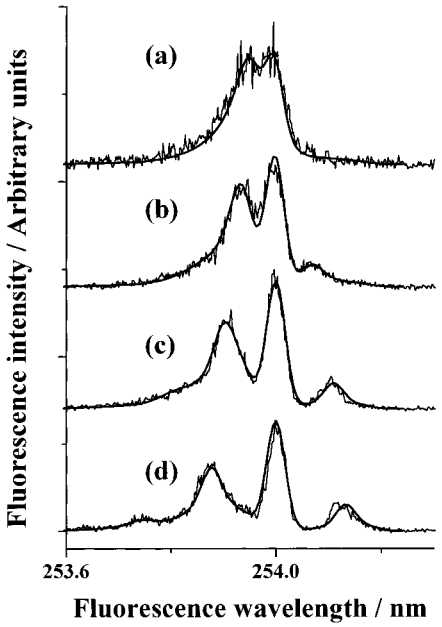

Figure 3. Directly returning SiF $C^2\Delta-X^2\Pi_{3/2}$ (0,0) fluorescence spectra following excitation of individual P_1 lines in the presence of H_2 (0.5 Torr) and Ar (1.4 Torr). Initially excited *j* levels are (a) 4.5, (b) 8.5, (c) 13.5, and (d) 16.5. The solid lines are best-fit simulations using adjustable rotational populations, as discussed in the text.

directly returning C−X fluorescence spectra. By excitation and observation, respectively, on the $^2\Delta-^2\Pi_{1/2}$ and $^2\Delta-^2\Pi_{3/2}$ subbands, which are separated by the relatively large spin−orbit splitting in the $X^2\Pi$ state, any potential interference from scattered pump-laser light was avoided. A sequence of such spectra produced by pumping on different rotational lines are shown in Figure 3. In all cases, the conditions were 0.5 Torr of H_2, 1.4 Torr of Ar, and trace amounts (∼1 mTorr) of SiF_4. The fluorescence in a 630 ns gate beginning just before the exciting laser pulse was collected. This comfortably exceeds the C state zero-pressure radiative lifetime of around 100 ns [34] and, more significantly, the measured fluorescence lifetime under these conditions (∼45 ns). The corresponding number of hard-sphere collisions suffered by an average SiF molecule prior to emission is calculated to be slightly less than 1.

If rotational equilibration had not been far from complete, the spectra in Figure 3 would have looked much more similar than the strongly contrasting appearance that they have in practice. Each of these spectra is characteristic of a distinctly non-Boltzmann distribution with a substantial component of the population in a single level (or at least narrow range of levels). There is nevertheless evidence for some rotational redistribution, with wings on the sharp features in the spectra that extend well beyond the bandwidth of the detection system. We are aided in detecting small changes in rotational state, despite the finite wavelength resolution, by spectroscopic details of the C−X transition. Each rotational level of the $C^2\Delta$ state is subject to spin-splitting into F_1 and F_2 levels: these would correspond either to the $^2\Delta_{3/2}$ and $^2\Delta_{5/2}$ manifolds of a Hund's case (a) state or to the $J = N \pm 1/2$ spin−rotation levels of a Hund's case (b) state.[37] The F_1 and F_2 levels are connected to the $X^2\Pi$ state by distinct spectroscopic branches, some of which are readily identifiable even in the absence of full rotational resolution.

The P_1 branch in the $^2\Delta-^2\Pi_{1/2}$ subband used to excite the C state prepares initially only F_1 levels. If there were no collisional transfer between F_1 and F_2 levels, the emission spectra on the $^2\Delta-^2\Pi_{3/2}$ subband in Figure 3 would contain only three branches ($^{Q}R_{12}$, $^{P}Q_{12}$, and $^{O}P_{12}$). However, quantitative fits, using a well-established procedure to calculate the rotational linestrengths,[38] were only satisfactory when the additional three branches (R_2, Q_2, and P_2) originating exclusively from collisionally populated F_2 levels were included. We therefore generated the fits shown in Figure 3 assuming that both the F_1 and F_2 manifolds were populated, each with an independently adjusted rotational distribution over the *j* levels. This represents a significant improvement over the less sophisticated assumption of unequally weighted but otherwise equivalent F_1 and F_2 population distributions in our previous preliminary report.[35] Trial distributions were adjusted iteratively until the visually assessed best-fit was achieved. The corresponding F_1 populations are plotted in Figure 4.

We conclude from the fits that the F_1 populations contain a large component (typically 40% of the F_1 population and hence 30% of the total) that remains in the initially populated level, superimposed on a relatively broad distribution spread over a range of adjacent *j*'s. In contrast, the F_2 levels were found to have only the broad component of the distribution. For levels other than the initially populated state, the spectra were best reproduced by assuming that F_1 and F_2 levels were unequally populated, with the F_1 levels favored by a factor of ∼2. This interesting propensity for retention of the spin label has not yet been examined in greater detail.

The highest *j* line we attempted to pump in state-specific transfer measurements corresponded to an initial *j* of 16.5. However, in this case only we found that it was not possible to generate a satisfactory fit to the experimental spectrum without including a secondary component, consisting of around 5% of the total population, in much higher rotational levels centered on $j = 58.5$. The discernible feature at ∼253.75 nm in the fluorescence spectrum in Figure 3d is associated entirely with this minor component. This is the result of accidental overlap of the pump laser with the corresponding high *j* line returning from the P_1 head,[39] highlighting the difficulties in exciting

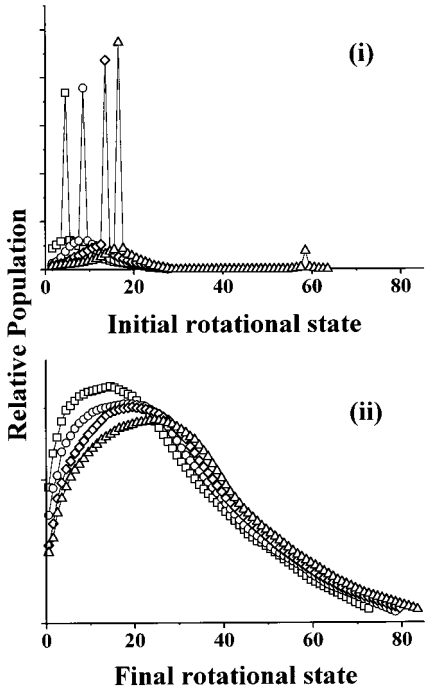

Figure 4. Best-fit SiF rotational population distributions with H_2 quencher. Part i shows the initial $C^2\Delta$, $v = 0$ populations, derived from the spectra in Figure 3. Only the F_1 populations are shown for the sake of clarity. Part ii shows product $B^2\Sigma^+$, $v' = 0$ populations, derived from the spectra in Figure 7. In both cases, the initially excited $C^2\Delta$ j level is indicated by the symbols: (□) 4.5; (○) 8.5; (◇) 13.5; (△) 16.5.

TABLE 1: Characteristics of the Initial Rotational State Distributions in SiF $C^2\Delta$, $v = 0$ Produced by Pumping Selected P_1 Branch Lines in the Presence of H_2 (0.5 Torr) and Ar (1.4 Torr)

j^a	$p_i{}^b$ (%)	F_1:$F_2{}^c$	$\langle j \rangle^d$	$j_{max}{}^e$
4.5	29	2.4	7.6	17.5
8.5	27	1.7	9.9	18.5
13.5	33	2.0	12.8	19.5
16.5	37	1.6	15.3[f]	20.5[f]

[a] $C^2\Delta$ state F_1 rotational level in which the exciting P_1 line terminated. [b] The fraction of the rotational population that remained in the pumped level, expressed as a percentage of the sum of populations in all F_1 and F_2 levels. [c] The ratio of collisionally produced F_1 to F_2 populations summed over all levels other than the one initially pumped. [d] The average rotational quantum number over the entire population of F_1 and F_2 levels. [e] The 95th percentile of the rotational distribution, i.e., the last j value for which the cumulative population is less than 95% of the total. [f] Excluding the minor high j component resulting from returning P_1 branch lines.

individual j states cleanly beyond the rather limited range we have included in this work. The quantitative characteristics of all the distributions for the different pump lines are collected in Table 1. For the purposes of comparison with $B^2\Sigma^+$ state product rotational distributions below, we have defined an operational maximum level j_{max} that can safely be said to be populated within the experimental signal-to-noise ratio. We have elected to take j_{max} to be the highest j value in the fit for which the cumulative population is less than 95% of the total.

As expected, dispersed C−X spectra recorded with longer integration gates under a given set of conditions (pressures of Ar and, for example, H_2) showed a slight progression toward larger fractions of redistributed rotational populations. However, increases in the pressure of an effective C state quencher, such as H_2, were found not to lead to much increase in the fraction of rotational redistribution. This is because the total quenching rate constant for these molecules is large,[34] and total removal therefore competes very effectively with rotationally inelastic processes within the C state. The principal effect of a high pressure of quencher is to greatly reduce the effective C state lifetime (see below) and therefore limit the number of rotationally inelastic collisions.

The results of this section confirm that pumping on different rotational lines successfully prepares distinct initial C state rotational populations, at least over a moderate range of rotational levels, which are only partially influenced by rotationally inelastic collisions. We therefore proceed below to use these distinct samples to investigate possible dependences of *inter*state transfer on initial rotational state.

3.3. Rotational Level Dependence of Total Removal from the C State. The zero-pressure radiative lifetime of the C state is around 100 ns.[34] Therefore, particularly at higher pressures of quencher, the correspondingly reduced fluorescence lifetimes do not greatly exceed the instrumental response time of our apparatus. The measured fluorescence decay profile $S(t)$, is expressible as a convolution integral

$$S(t) = \int_{-\infty}^{t} g(t')\, e^{-k(t-t')}\, dt' \qquad (1)$$

where $g(t')$ is the instrumental response function and k is the desired fluorescence decay constant (the reciprocal of the fluorescence lifetime). In the specific case that $g(t')$ is a Gaussian function centered at t_0 with a width parameter b, the convolution may be re-expressed as

$$S(t) = \int_{0}^{\infty} a\, e^{[-2(t-t_0-t')^2]/b^2}\, e^{-kt'}\, dt \qquad (2)$$

where a is an arbitrary scaling constant. This integral has the analytical solution[40]

$$S(t) = c\, e^{-k(t-t_0)}\left\{1 + \mathrm{erf}\left(\frac{\sqrt{2}}{b}\left(t - t_0 - k\left(\frac{b}{2}\right)^2\right)\right)\right\} \qquad (3)$$

where c is also a scaling constant.

Therefore, provided the instrumental response is well described by a Gaussian function, fluorescence decay constants can be derived from nonlinear least-squares fits[41] of eq 3 to the entire measured fluorescence decay, including the rising edge. This eliminates some of the difficulties with a less refined analysis, such as, for example, having to choose arbitrarily a fraction of the decaying portion of the profile to be fitted with a simple exponential function.[34]

The reasonable fit of a Gaussian function to our measured scattered laser light signal is illustrated in Figure 5. The fitted value of the width parameter b was reproducibly around 20−25 ns, reflecting the combined effects of the laser pulse length, the response time of the PMT, and the analog bandwidths of the preamplifier and transient digitizer.

We systematically investigated the quality and reproducibility of fits of eq 3 to entire SiF C−X (0,0) fluorescence decay profiles, which were free from scattered laser light through being excited and observed on different subbands (see section 3.2), using several excitation lines in the P_1 branch. We alternatively treated b as a free parameter or constrained it to the value determined independently from the fit to the scattered laser light. We quite generally found no numerically significant differences in the k values from the two methods, although, unsurprisingly, a free b gave slightly better overall fits. We also compared the values obtained by fitting a simple exponential to selected decaying portions of the profile and typically found k to be

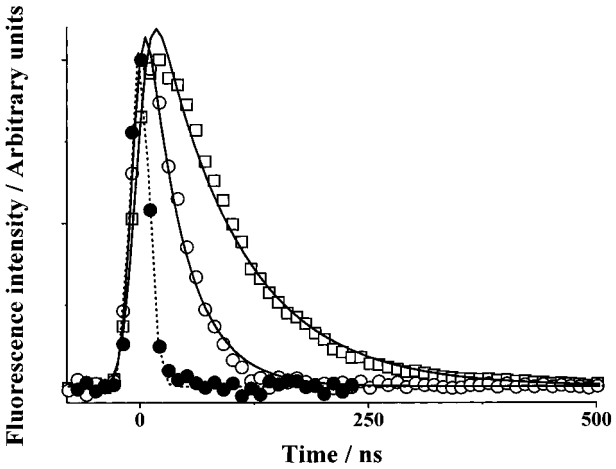

Figure 5. Representative SiF C−X (0,0) fluorescence decay curves for a fixed pressure (1.5 Torr) of Ar carrier and two different pressures of H_2: (□) 0.63 Torr; (○) 0.85 Torr. The solid lines are best-fits of eq 3. The much shorter profile (●) is the instrumentally limited scattered laser light signal (not present in the other signals) through which the dashed line is the best-fit to a Gaussian function.

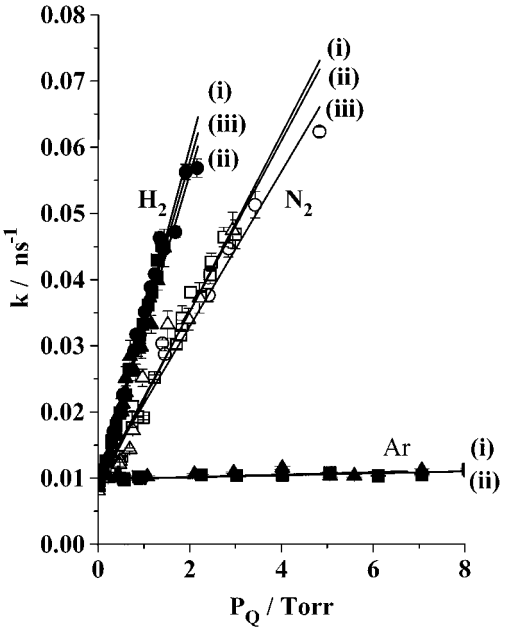

Figure 6. Variation of the SiF $C^2\Delta$, $v = 0$ fluorescence decay constant k with pressure of different quenchers, as indicated, and for several initial rotational levels: (i) and triangles, $j = 2.5$; (ii) and squares, $j = 11.5$; (iii) and circles, $j = 21.5$.

smaller by ∼10%. Representative fits to measured profiles with different pressures of H_2 quencher are included in Figure 5.

The resulting values of k may then be plotted against the pressure of quencher, P_Q, in the usual way, to yield the j-specific total quenching rate constants k_Q^j:

$$k = (1/\tau_{rad}^j) + k_Q^j P_Q \qquad (4)$$

where τ_{rad}^j is the (in principle) j-dependent zero-pressure radiative lifetime. Plots for the j levels we have examined are shown in Figure 6, and the numerical results are collected in Table 2. It is apparent that there is little, if any, statistically significant variation in k_Q^j with the initially pumped value of j in the range 2.5−21.5 for the quenchers investigated (H_2, N_2, and less extensively, Ar). These phenomenological measurements also reflect any true dependence of the efficiency of total quenching

TABLE 2: Fitted Values and Uncertainties (1σ) of Rotational Level-Specific Total Quenching Rate Constants, k_Q^j, and Zero-Pressure Radiative Lifetimes τ_{rad}^j, for SiF $C^2\Delta$, $v = 0$

			$k_Q^j/10^{-11}$ molecule^{-1} cm^3 s^{-1}	
j[a]	quencher	τ_{rad}^j/ns	this work	previously[c]
2.5	H_2	112 ± 7	72.8 ± 2.3	116 ± 12
11.5		123 ± 7	80.3 ± 1.5	
21.5[b]		104 ± 6	74.8 ± 1.7	
2.5	N_2	118 ± 10	41.4 ± 1.9	23.4 ± 2.4
11.5		108 ± 5	40.0 ± 0.9	
21.5[b]		105 ± 7	36.2 ± 1.1	
2.5	Ar	101.9 ± 2.5	0.55 ± 0.20	
11.5		101.7 ± 1.2	0.44 ± 0.09	*d*

[a] $C^2\Delta$ state F_1 rotational level in which the exciting P_1 line terminated. Some population would be redistributed by rotationally inelastic collisions, as discussed in section 3.2. [b] A minor, higher j component would also be excited in conjunction with $j = 21.5$, owing to underlying lines returning from the P_1 head, in a way similar to that discussed in section 3.2. [c] Reference 34. The initial j level was not selected in that work. [d] Quenching by Ar was too slow to be measured within the precision of the measurements in ref 34.

on j to the extent that the rotational populations are not collisionally thermalized, as discussed at length in section 3.2. Although these interfering effects may be sufficient to obscure a weak j dependence, we do not believe they are themselves responsible for the apparent similarity in the observed quenching rate constants.

The present k_Q^j values differ somewhat from those reported for H_2 and N_2 in the previous[34] rotationally nonselective investigation. We believe this disagreement is primarily the result of the recalibration of the flow characteristics of the apparatus, and therefore that the current values are likely to be significantly more accurate. The improved precision has also allowed us to report a finite quenching rate constant for Ar for the first time.

The zero-pressure radiative lifetimes τ_{rad}^j are also essentially independent of j. The most accurate values are likely to be those derived from the Ar-only measurements because of the very weak pressure dependence. An average lifetime of 101.8 ± 1.4 ns for the lower j levels disagrees only slightly with the previously reported[34] value of 94 ± 2 ns.

3.4. C-B Interstate Inelastic Processes. *3.4.1. Dependence of Vibronic Branching on Initial Rotational State.* The most straightforward way to produce relatively large differences in the initial C state rotational distribution is to pump at the Q_1 and P_1 bandheads, as in our previous work.[35] This creates distributions that peak at j values around 11.5 and 34.5, respectively.

We have recorded additional vibronically resolved fluorescence spectra, covering the region from 250 to 320 nm containing both C−X and B−X bands,[36] following excitation of the $C^2\Delta$, $v = 0$ level at each of the Q_1 and P_1 heads. Within the experimental signal-to-noise ratio, the spectra excited at each head were identical for a given quencher (either H_2 or N_2), both in terms of the ratio of C−X to B−X emission and in the pattern of B−X vibronic bands. These results establish that there is no significant (within ∼5% for H_2 and ∼25% for N_2) influence of this change in the initial rotational state distribution on f_B, the electronic branching fraction for specific transfer to the $B^2\Sigma^+$ state. There is a similar lack of dependence of the vibrational distribution in the $B^2\Sigma^+$ state.

Given these results for the relatively large changes in rotational state achieved by pumping at the different heads, we did not consider it worthwhile to look for the weak (if any)

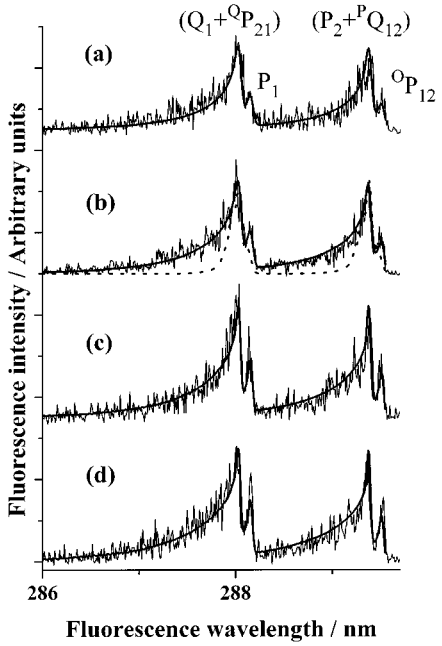

Figure 7. SiF B−X (0,0) fluorescence spectra resulting from collisions of $C^2\Delta$, $v = 0$ with H_2. The initially excited C state rotational level j was as in Figure 3: (a) 4.5; (b) 8.5; (c) 13.5; (d) 16.5. The solid lines are best-fit simulations using the B-state rotational populations shown in Figure 4ii. The dashed line in (b) is an indication of the spectrum that would have been observed if $\Delta j = 0$ during the collision-induced transition.

variations that we would expect following more selective excitation to individual rotational levels.

3.4.2. Dependence of B State Rotational Distribution on Initial Rotational State. More highly dispersed B−X (0,0) fluorescence spectra, which are sufficiently resolved to reveal at least the contours of the B-state rotational populations, are shown in Figure 7. These collision-induced spectra were obtained following excitation of individual P_1 lines in the C−X (0,0) band in the presence of H_2 quencher, under conditions similar to those of the directly returning C−X fluorescence spectra in Figure 3. We reiterate the point stressed in our earlier work[34,35] that because the B-state radiative lifetime is at least an order of magnitude shorter than that of the C state, there is effectively no secondary collisional redistribution of B-state rotational populations under these conditions.

The solid lines in Figure 7 represent best-fit simulations, using calculated line strengths[38] and adjustable $B^2\Sigma^+$, $v' = 0$ rotational populations. The experimental spectra were reproduced satisfactorily if it was assumed that the spin−rotation (F_1 and F_2) levels in the B state were equally populated. The corresponding B-state rotational distributions are compared in Figure 4 with those of the C state from which they are produced. The numerical characteristics of the product distributions are listed in Table 3.

Because of the finite wavelength resolution and signal-to-noise ratio of the experimental spectra, there is inevitably some flexibility in the B-state distributions that will give satisfactory fits. In particular, it is difficult to establish conclusively the location of the peak of a relatively broad distribution, of the high j' tail where the corresponding signals become comparable with the noise, and the relative populations of the lowest few levels for which the lines are congested beneath the bandwidth of the detection system. Operationally, an initial $B^2\Sigma^+$ state distribution was selected with a single maximum and no inflections, going smoothly to zero at high j'. This was then iteratively adjusted, avoiding unnatural sharp discontinuities or inflections, until satisfactory "by eye" agreement with experimental results was obtained. In line with the definition for j_{max} introduced for the initial C-state distribution above, we have quoted equivalent j'_{max} values in Table 3.

TABLE 3: Characteristics of SiF $B^2\Sigma^+$, $v' = 0$ Rotational State Distributions Produced in Collisions of Rotationally State-selected $C^2\Delta$, v=0 with H_2

j[a]	$\langle j' \rangle$[b]	$\langle \Delta j \rangle$[c]	j'_{max}[d]	Δj_{max}[e]
4.5	24.9	17.3	56.5	39
8.5	26.9	17.0	59.5	41
13.5	28.4	15.6	61.5	42
16.5	30.2	14.9[f]	64.5	44[f]

[a] $C^2\Delta$ state F_1 rotational level in which the exciting P_1 line terminated, as in Table 1. [b] Average rotational quantum number in the collisionally produced $B^2\Sigma^+$, $v' = 0$ level. [c] Average change in rotational quantum number between the $B^2\Sigma^+$, $v' = 0$ product distribution and the corresponding $C^2\Delta$, $v = 0$ distribution from which it was collisionally produced, i.e., $\langle \Delta j \rangle = \langle j' \rangle - \langle j \rangle$. [d] The 95th percentile of the $B^2\Sigma^+$, $v' = 0$ product rotational distribution, i.e., the last j' value for which the cumulative population is less than 95% of the total. [e] The difference between 95th percentiles of the $B^2\Sigma^+$, $v' = 0$ and $C^2\Delta$, $v = 0$ rotational distributions, i.e., $\Delta j_{max} = j'_{max} - j_{max}$. [f] Neglecting the high j component of the $C^2\Delta$, $v = 0$ population. See note f in Table 1 and the discussion in section 3.2 of the text.

Despite these limitations, the general features of the distribution, such as the width and average, are well determined. In particular, there is no doubt that the product B-state rotational distributions are *very substantially broader* than the initial C-state distribution. This point is illustrated in Figure 7b, where a simulation is also shown that corresponds to the spectrum that would have been obtained if the B-state distribution had been identical with the C-state distribution from which it was collisionally produced. Clearly, this is a very poor fit to the experimental B−X spectrum.

There is also, perhaps less obviously, a definite correlation between the experimental B−X spectra and the initial C-state populations from which each is produced. One visible effect of this is a systematic variation in Figure 7 in the ratio of the major to minor heads ($Q_1 + {}^QP_{21}$ to P_1 in the $^2\Sigma^+ - {}^2\Pi_{1/2}$ subband and $P_2 + {}^PQ_{12}$ to ${}^OP_{12}$ in the $^2\Sigma^+ - {}^2\Pi_{3/2}$ subband). Because the $Q_1 + {}^QP_{21}$ and $P_2 + {}^PQ_{12}$ heads form at relatively low levels ($j' \approx 6.5$) in comparison to the corresponding P_1 and ${}^OP_{12}$ heads ($j' \approx 19.5$), a change in the ratio reflects a shift in population from low to medium j', consistent with the best-fit distributions in Figure 4ii.

4. Discussion

Any consistent mechanism for the quenching of SiF $C^2\Delta$, and in particular the specific channel transferring population to the $B^2\Sigma^+$ state, must simultaneously explain the principal features of the experimental observations in this work and previous studies.[34,35] In summary, we find that regardless of the collision partner there is a relatively moderate, if any, influence of initial SiF rotational state on the probability of quenching, on the electronic branching fraction, and on the product vibrational distribution. In contrast, the initial rotational angular momentum adds to the substantial SiF product rotational motion that is created in state-changing collisions. The identity of the partner does affect the product rotational distributions significantly.[35] The remaining energy is partitioned largely to translation, with a relatively cold vibrational distribution reflecting the Franck−Condon overlap between initial and final vibrational wave functions, relatively independent of the collision partner.[34]

The lack of any strong *j* dependence on the various properties other than the product rotational distribution suggests that there is no particularly preferred geometry for collision-induced transfer out of the $C^2\Delta$ state. Otherwise, a well-established argument suggests that increased initial rotational motion will tend to disrupt the preferred geometry and therefore cause a decrease in the quenching probability. The absence of any strong steric constraints is also consistent with the large absolute values for the total quenching rate constants.

The very significant product rotational excitation is certainly one of the most remarkable aspects of these results. As noted in the Introduction, this is by no means a common feature of collision-induced electronic state-changing processes. The extent to which it is particularly unexpected in SiF···H_2 collisions emerges from an (over-) simplified consideration of kinematics. Neglecting any initial translational and rotational energy of the collision partners, the total energy available to the products of a collision-induced transition from SiF $C^2\Delta$, $v = 0$ to $B^2\Sigma^+$, $v' = 0$ is around 5000 cm^{-1} (see Figure 1). In the extreme limit of an impulse acting between two spherical particles with the relative masses of SiF and H_2, momentum conservation requires that the lighter H_2 particle should carry away a fractional share of ~47/49 of the available energy. Even if all the remaining energy (only ~200 cm^{-1}) were somehow converted to SiF rotation, this would be nowhere near sufficient to populate the high j' levels that are observed experimentally!

A more realistic model would recognize from the start that the SiF molecule is not spherical. In some perpendicular geometries with nonzero impact parameters relative to the SiF center of mass, the H_2 molecule would effectively feel an impulse from only one end of the molecule. The rotational motion in SiF would be optimized if this was the lighter F-atom end. Roughly speaking, the simple kinematic argument above, modified for mutual F···H_2 repulsion, suggests that ~500 cm^{-1} could be converted to SiF product rotation. This is still very well short of the energies of the higher j' levels seen experimentally.

It is clear that oversimplified kinematic arguments based on repulsion between initially static SiF···H_2 collision pairs are not capable of explaining the experimental observations. We have therefore developed a more refined model for the prediction of the *maximum* product rotational level. This correctly includes three distinct sources of SiF product angular momentum j'. These are, respectively, addition of the initial SiF rotational angular momentum j, conversion of initial linear momentum of the collision pair to j', and conversion of the released electronic energy, ΔE, to j'. The last two contributions are a result of forces that act along a line that does not pass through the SiF center-of-mass and therefore impart a torque. We have previously presented[35] an outline of this model and brief consequences of its results, but we now discuss it in greater detail.

The solution to the simpler problem of a rotational state-changing collision *within* a single electronic state, where there is no additional electronic energy defect, ΔE, to be distributed, is well-known.[42] Proceeding in a similar vein, we treat the SiF molecule as a "hard-shape" and the collision partner as a "hard-sphere". For each point on the perimeter of the hard shape there is an extrapolated normal that, in general, does not pass through the center-of-mass. The perpendicular distance from this normal to the center-of-mass defines the lever arm (an effective impact parameter *b*) and hence the torque imparted by an impulse at the surface. Assuming that the electronic energy release and the conversion of linear to angular momentum both occur suddenly at the instant that contact takes place between the bodies, the same value of *b* applies to both these processes. The maximum value of *b* is labeled b_{max}.

The *maximum* change in rotational state, Δj_{max}, will occur when the initial angular momentum vector **j** happens to be perpendicular to the plane containing the SiF center-of-mass and the point of contact, and the initial linear momentum **p** is along the surface normal. In other words, the initial orbital, **l**, and rotational, **j**, angular momentum vectors are parallel before the collision. After the collision, **j′** remains parallel to **j**, but its magnitude is significantly increased. Angular momentum is conserved by the contribution from **l′** because **p′** is in the opposite direction to **p** for a rebound collision.

Proceeding mathematically to a solution for this particular case, the system must simultaneously satisfy energy conservation

$$\frac{p^2}{2\mu} + \frac{\hbar^2 j^2}{2I} + \Delta E = \frac{p'^2}{2\mu} + \frac{\hbar^2 j'^2}{2I} \tag{5}$$

and conservation of angular momentum

$$\hbar j + p b_{max} = j' - p' b_{max} \tag{6}$$

where μ is the reduced mass of the collision pair and *I* is the moment of inertia of the hard shape. Elimination of p' from eq 5 using eq 6 and of j' through the relation $j' = j + \Delta j_{max}$ leads to a quadratic equation for Δj_{max}. The desired solution is the more positive root, which has the value

$$\Delta j_{max} = \frac{b_{max}}{\hbar(1+\eta)}\{\alpha + [\alpha^2 + 2\mu\Delta E(1+\eta)]^{1/2}\} \tag{7}$$

where η is defined by

$$\eta = \frac{\mu b_{max}^2}{I} \tag{8}$$

and α by

$$\alpha = p - \frac{\hbar\mu b_{max} j}{I} \tag{9}$$

When attempting to model a particular system using eq 7, the principal unknown quantity is the value of b_{max}. In their closely related (and more developed) modeling of rotational energy transfer *within* single electronic states of homonuclear diatomics, McCaffery and co-workers[43,44] have consistently found that the equivalent b_{max} parameter had a physically reasonable value close to half the homonuclear bond distance. In the present case of a heteronuclear diatomic, we suggest correspondingly that b_{max} is unlikely to significantly exceed the average distance of 0.92 Å between the F nucleus and the SiF center-of-mass in the $C^2\Delta$, $v = 0$ level.

Taking this value for b_{max}, we demonstrate in Figure 8 the *j* dependence of the relative contributions to Δj_{max} from the sources identified above. The mass parameters are specific to SiF···H_2 collisions except for the uppermost trace (open symbols), which is for SiF···N_2 (see below). The lowest trace illustrates the relatively modest rotational release that could be achieved if there were no rovibronic energy defect, i.e., $\Delta E = 0$, and the relative collision velocity is taken to be the thermal average ($\langle v_{rel} \rangle$ = 1820 ms^{-1} at 300 K). These Δj_{max} values decline approximately linearly with *j* (reflecting the nonlinear relationship between rotational quantum number and energy).

The middle four traces (solid lines) represent SiF···H_2 collisions with the correct value of ΔE for $C^2\Delta$, $v = 0$ to $B^2\Sigma^+$,

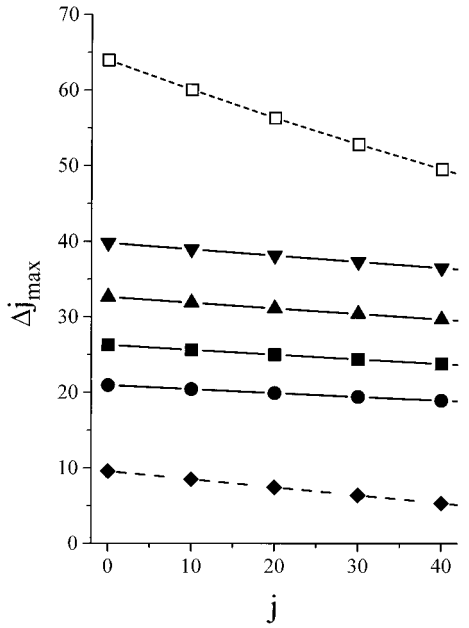

Figure 8. Predicted maximum changes in rotational state Δj_{max} as a function of initial SiF rotational level j using an impulsive model (eq 7) for SiF···quencher collisions. In all cases $b_{max} = 0.92$ Å. All filled symbols are for H_2 quencher. Solid lines represent $\Delta E = 4816$ cm^{-1}, with collision velocities v equal to multiples of the average thermal relative velocity $\langle v_{rel} \rangle = 1820$ ms^{-1}: (●) v=0; (■) $v = \langle v_{rel} \rangle$; (▲) $v = 2\langle v_{rel} \rangle$; (▼) $v = 3\langle v_{rel} \rangle$. Long-dashed line and ◆ are for $\Delta E = 0$ and $v = \langle v_{rel} \rangle$. Short-dashed line and □ are for N_2 quencher, $\Delta E = 4816$ cm^{-1}, and $v = \langle v_{rel} \rangle = 602$ ms^{-1}.

$v' = 0$ transfer. Successive multiples of $\langle v_{rel} \rangle$ have been taken to illustrate the effects of varying the collision velocity. The Δj_{max} values from ΔE alone with no initial linear momentum are significantly larger, and decline less rapidly with j, than those with $\Delta E = 0$ and the average thermal velocity. As should be expected, increasing the initial relative velocity produces proportional further increases in Δj_{max}, with an approximately constant additional increase due to **l** to **j′** conversion on top of the weakly j-dependent rotation resulting from ΔE alone.

These absolute values for Δj_{max} are clearly much larger than those implied by the oversimplified kinematic analysis made above. The physical reason for this is that in collisions that lead to the maximum product rotation, the F atom is receding from the approaching H_2 molecule in the laboratory frame because of the initial SiF rotational motion. After the collision the recoiling H_2 is moving rapidly relative to the F atom but relatively more slowly in the laboratory frame, therefore absorbing much less energy in relative translation than was crudely estimated above.

The Δj_{max} values required to match experiment for SiF···H_2 are ~40 (see Table 3 and Figure 4), although we reiterate the difficulties in defining exactly the highest levels that are populated experimentally (see section 3.4.2). It seems clear that only the higher assumed velocities are capable of producing realistic predictions of Δj_{max}. We note that velocities of 1, 2, and 3 times $\langle v_{rel} \rangle$ would be exceeded in around 60%, 4%, and 0.01% of collisions, respectively (including the weighting of the rate of collisions by the velocity). We conclude that the experimentally observed values of Δj_{max} are being approached as the relative velocity is increased toward the high-velocity tail of a thermal sample. Agreement could also be improved for lower collision velocities by increasing b_{max} because the leading term in eq 7 produces approximately linear variations in Δj_{max}, but we are reluctant to believe that much larger values are physically probable.

Most of the assumptions we have introduced, such as the suddenness of the interaction and the likely value of b_{max}, will produce an upper limit on the product rotational motion. We believe this indicates that, regardless of the limitations of the current model, there must be a very strongly repulsive interaction between SiF and H_2 at the instant of the collision-induced electronic transition and that some of these collisions must occur through substantially bent geometries.

A further respect in which we believe that our cumulative results support an impulsive mechanism is the previous observation[35] that the level of rotational excitation in the product SiF is greater for N_2 quencher than for H_2. This is consistent with the impulsive kinematics discussed above and is reproduced in the results of eq 7 as included in Figure 8. The Δj_{max} values are shown for SiF···N_2 collisions (uppermost trace, open symbols) with the thermal average collision velocity of 602 ms^{-1} and the same assumed b_{max} of 0.92 Å. The predictions for N_2 are comfortably able to explain the experimental estimates[35] of $\Delta j_{max} \approx 50$. More caution should probably be exercised in applying this model with N_2 than with H_2 as the "hard sphere". Because of its low moment of inertia and correspondingly large rotational constant, H_2 is precluded from carrying away a substantial component of angular momentum following the collision. Although this is no longer true for N_2, the homonuclear N_2 molecule should appear substantially less electronically anisotropic than the SiF collision partner. It is therefore reasonable that N_2 should be less rotationally excited in a collision, and treating it as a hard-sphere is not too extreme an assumption.

We note that in some other mechanisms, such as those involving statistical distributions over available product states conventionally associated with long-lived collision complexes, the SiF product would be predicted to be *less* rotationally excited for N_2 than for H_2. This is because, at least in a simple "prior" distribution,[45] a given energy in rotation has a higher degeneracy and hence associated statistical weight for N_2 than for H_2, consequently reducing the energy available for SiF rotation. Consistently, we have also argued previously[34,35] that the observed Franck−Condon control of the SiF product *vibrational* distributions is characteristic of a sudden process and not of the statistical redistribution of energy in a long-lived complex.

A key final question is therefore why should the SiF $C^2\Delta - B^2\Sigma^+$ system exhibit this behavior, indicative of a strongly repulsive interaction leading to translational and rotational energy release, which is atypical[1] of the majority of collision-induced electronic transitions? We believe the answer lies, as we have stated previously,[34,35] in the valence to Rydberg character of the collision-induced transition. The basic idea is that the outermost electrons in the $C^2\Delta$ state, known to have predominantly valence character, occupy a much smaller volume than the outer Rydberg electron in the $B^2\Sigma^+$ state, which is effectively in a Si 4s atomic orbital.[36] Therefore, when the collision partner has penetrated sufficiently close to induce the electronic transition, at a distance that may be at most mildly repulsive on the $C^2\Delta$ state potential energy hypersurface, a very large instantaneous repulsion is experienced on the nascent $B^2\Sigma^+$ state surface.

This argument is closely analogous to the known[46−48] strong blue shift of transitions to low-lying molecular Rydberg states relative to those to excited valence states in low-temperature solid matrixes. To put it on a slightly more quantitative footing in the present case, we can compare measures of the size of the Si 3p valence orbitals (which make a dominant contribution to the highest-occupied SiF π^* valence orbitals in the $C^2\Delta$ state)

and the Si 4s orbital. The average distance of a valence electron from the nucleus is given approximately by[49,50]

$$\bar{r} \approx \frac{n^2 a_0}{Z^*} \tag{10}$$

where n is the principal quantum number, a_0 is the Bohr radius, and Z^* is an effective nuclear charge including the effects of screening by inner electrons. The standard Slater's rules allow Z^* to be estimated,[50] with a resultant radius of 1.15 Å for the Si 3p orbital.

Similarly, for a hydrogen-like Rydberg orbital, the radius can be obtained from

$$\bar{r} \approx n^{*2} a_0 \tag{11}$$

where n^* is an effective quantum number that differs from n by the quantum defect d; i.e., $n^* = n - d$. Quantum defects may be deduced directly from experimentally observed term energies and ionization potentials. For both the bare Si 4s Rydberg atom and the SiF $B^2\Sigma^+$ state, d has a value[51] around 1.9. The corresponding radius of the orbital is 2.4 Å, roughly twice that of the 3p valence orbital, lending quantitative support to the qualitative arguments above.

5. Principal Conclusions

The rotational angular momentum of SiF $C^2\Delta$ has little effect on the rate of total quenching by simple partners. It also does not influence the fraction of the quenched molecules that are deposited in the $B^2\Sigma^+$ state or the vibrational distribution within this state. It does, however, add to the sizable rotational angular momentum that is generated in the $B^2\Sigma^+$ state as a consequence of the electronic state change. These results are consistent with a strongly repulsive mechanism for the disposal of the electronic energy, which we believe to be a consequence of the valence to Rydberg character of the collision-induced transition.

Acknowledgment. Dr. C. W. Watson and Miss E. Scott made technical contributions to the experiments and data analysis. We are grateful to the EPSRC for an equipment grant and studentships for N.J. and C.R. and to Shell Research Ltd for further financial support.

References and Notes

(1) Dagdigian, P. J. *Annu. Rev. Phys. Chem.*, in press.
(2) Katayama, D. H. *J. Chem. Phys.* **1984**, *81*, 3495.
(3) Katayama, D. H. *Phys. Rev. Lett.* **1985**, *54*, 657.
(4) Katayama, D. H.; Dentamaro, A. V. *J. Chem. Phys.* **1986**, *85*, 2595.
(5) Katayama, D. H.; Dentamaro, A. V.; Welsh, J. A. *J. Chem. Phys.* **1987**, *87*, 6983.
(6) Katayama, D. H.; Dentamaro, A. V. *J. Chem. Phys.* **1989**, *91*, 4571.
(7) Dentamaro, A. V.; Katayama, D. H. *Phys. Rev. A.* **1991**, *43*, 1306.
(8) Katayama, D. H.; Miller, T. A.; Bondybey, V. E. *J. Chem. Phys.* **1979**, *71*, 1662.
(9) Furio, N.; Ali, A.; Dagdigian, P. J. *Chem. Phys. Lett.* **1986**, *125*, 561.
(10) Furio, N.; Ali, A.; Dagdigian, P. J. *J. Chem. Phys.* **1986**, *85*, 3860.
(11) Jihua, G.; Ali, A.; Dagdigian, P. J. *J. Chem. Phys.* **1986**, *85*, 7098.
(12) Ali, A.; Jihua, G.; Dagdigian, P. J. *J. Chem. Phys.* **1987**, *87*, 2045.
(13) Dagdigian, P. J.; Patel-Misra, D.; Berning, A.; Werner, H.-J.; Alexander, M. H. *J. Chem. Phys.* **1993**, *98*, 8580.
(14) Fei, S.; Heaven, M. C. *J. Chem. Phys.* **1993**, *98*, 753.
(15) Lin, H.-S.; Erickson, M. G.; Lin, Y.; Basinger, W. H.; Lawrence, W. G.; Heaven, M. C. *Chem. Phys.* **1994**, *189*, 235.
(16) de Moor, M.; Ottinger, Ch.; Vilesov, A. F.; Xu, D. D. *J. Chem. Phys.* **1994**, *101*, 9506.
(17) Bondybey, V. E.; Miller, T. A. *J. Chem. Phys.* **1978**, *69*, 3597.
(18) Katayama, D. H.; Welsh, J. A. *J. Chem. Phys.* **1983**, *79*, 3627.
(19) Katayama, D. H.; Welsh, J. A. *Chem. Phys. Lett.* **1984**, *106*, 74.
(20) Dentamaro, A. V.; Katayama, D. H. *J. Chem. Phys.* **1989**, *90*, 91.
(21) Dentamaro, A. V.; Katayama, D. H. *J. Chem. Phys.* **1994**, *101*, 8628.
(22) Alexander, M. H.; Corey, G. C. *J. Chem. Phys.* **1986**, *84*, 100.
(23) Werner, H.-J.; Follmeg, B.; Alexander, M. H. *J. Chem. Phys.* **1988**, *89*, 3139.
(24) Werner, H.-J.; Follmeg, B.; Alexander, M. H.; Lemoine, D. *J. Chem. Phys.* **1989**, *91*, 5425.
(25) Berning, A.; Werner, H.-J. *J. Chem. Phys.* **1994**, *100*, 1953.
(26) Adams, J. S.; Pasternack, L. *J. Phys. Chem.* **1991**, *95*, 2975.
(27) Hack, W.; Rathman, K. *J. Phys. Chem.* **1992**, *96*, 47.
(28) Patel-Misra, D.; Dagdigian, P. J. *J. Chem. Phys.* **1992**, *97*, 4871.
(29) Hussein, K.; Aubert-Frécon, M.; Babaky, O.; D'Incan, J.; Effantin, C.; Vergès, J. *J. Mol. Spectrosc.* **1985**, *114*, 105.
(30) Astill, A. G.; McCaffery, A. J.; Taylor, S. C.; Whitaker, B. J.; Wynn, M. J. *J. Chem. Phys.* **1988**, *89*, 184.
(31) Rohrer, F.; Stuhl, F. *J. Chem. Phys.* **1987**, *86*, 226.
(32) Jeffries, J. B. *J. Chem. Phys.* **1991**, *95*, 1628.
(33) Singleton, S.; McKendrick, K. G. *J. Phys. Chem.* **1993**, *97*, 1389.
(34) Watson, C. W.; McKendrick, K. G. *Chem. Phys.* **1994**, *187*, 79.
(35) Jackson, N. A.; Watson, C. W.; McKendrick, K. G. *Chem. Phys. Lett.* **1995**, *243*, 564.
(36) Watson, C. W.; McKendrick, K. G. *Chem. Phys.* **1994**, *187*, 87.
(37) The numerical value of the SiF $C^2\Delta$ state spin−orbit coupling constant, A, is the subject of an interesting spectroscopic curiosity [Houbrechts, Y.; Dubois, I.; Bredohl, H. *J. Phys. B: At. Mol. Phys.* **1980**, *13*, 3369]. Equivalent term value expressions are obtained (for all but the unique, lowest Λ-doubled level) with either $A = 0$ or $A = 4B$, where B is the rotational constant. Spectral congestion has prevented these cases from being distinguished by observing the frequencies of the only three lines within this subband that are not the same for these two values of A. However, our own results for the relative *intensities* of resolved, low-j lines in the P_1 branch of the LIF excitation spectrum suggest a better match to those simulated [see ref 38] with a value of $A = 2.46$ cm^{-1} ($\sim 4B$) than to those with $A = 0$. Regardless of which of these two relatively small values of A is correct, the SiF C state will rapidly approach the Hund's case (b) coupling limit with increasing rotational level.
(38) A computer code for the calculation of transition frequencies and rotational linestrengths in electronic spectra was kindly supplied by Professor R. N. Zare, which is based on an extension of the methods described in the following. Zare, R. N.; Schmeltekopf, A. L.; Harrop, W. J.; Albritton, D. L. *J. Mol. Spectrosc.* **1973**, *46*, 37.
(39) We used the published molecular constants [see ref 36] to calculate the rotational levels for which the lines should be accidentally resonant in outward and returning limbs of the P_1 branch of the excitation spectrum. The prediction was that those terminating in $j = 16.5$ and 54.5 should overlap. However, when we used the same constants to simulate our observed fluorescence spectra, it was clear that the minor higher j component was displaced slightly from the predicted wavelengths in the $^PQ_{12}$ branch in which its presence is most apparent. Operationally, we were able to obtain a satisfactory simulation of the fluorescence spectra without adjusting the constants but by assuming that the minor high j component was located at $j = 58.5$. This slight uncertainty in the true j values of the high j component has no significant effect in the present context on the interpretation of the spectra.
(40) Abramovitz, M., Stegun, I. A., Eds., *Handbook of Mathematical Functions*; Dover Publications: New York, 1965; p 302.
(41) Bevington, P. R. *Data Reduction and Error Analysis for the Physical Sciences*; McGraw-Hill: New York, 1969; p 204.
(42) Murrell, J. N., Bosanac, S. D., *Introduction to the Theory of Atomic and Molecular Collisions*; Wiley: New York, 1989; p 79.
(43) Osborne, M. A.; McCaffery, A. J. *J. Chem. Phys.* **1994**, *101*, 5604.
(44) Osborne, M. A.; Marks, A. J.; McCaffery, A. J. *J. Phys. Chem.* **1996**, *100*, 3888.
(45) Levine, R. D.; Bernstein, R. B. *Molecular Reaction Dynamics and Chemical Reactivity*; Oxford University Press: New York, 1987; p 274.
(46) Herzberg, G.; Lagerqvist, A.; Miescher, E. *Can. J. Phys.* **1956**, *34*, 622.
(47) Lagerqvist, A.; Miescher, E. *Helv. Phys. Acta* **1958**, *31*, 221.
(48) Lagerqvist, A.; Miescher, E. *Can. J. Phys.* **1962**, *40*, 352.
(49) Pauling, L.; Wilson, E. B. *Introduction to Quantum Mechanics*; McGraw-Hill: New York, 1935; p 144.
(50) Jean, Y.; Volatron, F.; Burdett, J. *An Introduction to Molecular Orbitals*; Oxford University Press: New York, 1993; p 54.
(51) Bosser, G.; Bredohl, H.; Dubois, I. *J. Mol. Spectrosc.* **1984**, *106*, 72.